A CCD Miniature Radiation Monitor[1]

A. M. Chugg[2], R. Jones[2], P. Jones[2], P. Nieminen[3], A. Mohammadzadeh[3], M. S. Robbins[4], K. Lovell[5]

Abstract

A miniature radiation monitor (MRM) device has been developed, which utilises a CCD as its sensitive element. Its shielding configuration has been designed to mitigate the displacement damage threat in space environments, whilst also introducing a good degree of directional sensitivity.

I. INTRODUCTION

The objective of the project has been to design and develop a miniature radiation monitor for spacecraft applications which provides a comparable range of radiation environment data to existing instruments, but at around an order of magnitude lower power consumption, mass and volume and a lower unit cost. In order to achieve such ambitious targets, it was considered desirable to obtain all the requisite types of radiation measurement from a single sensitive device. Previous work by the MBDA Radiation Effects Group [1] and others [2] had shown that a CCD device has the ability to count individual charged radiation particles and to distinguish between species based on the widely varying ranges of signal deposited in a struck pixel due to differing particle LET's. Proton and electron environments can therefore be measured simultaneously but distinctly by a single array.

Many existing CCD's perform adequately at total doses up to ~20krads and it is possible to harden CCD's to total doses of 1Mrad and above. However, the very high natural levels of displacement damage experienced in most Earth orbits constitute a major impediment to the concept [3], [4]. Unless very heavily shielded, a CCD will rapidly be destroyed by this environment (relative to the durations of most missions). Conversely, sufficient shielding to protect against displacement damage from high energy protons would normally render the electron environment invisible to the CCD. Evidently, what is required is a heavy shielding configuration, which nevertheless admits a sample of the raw space radiation environment and somehow dilutes it by a factor of ~100 across the surface of the CCD device. Just such a configuration is created by a double-conical pinhole aperture. Furthermore, such an aperture will engender a high degree of directional sensitivity in the radiation distribution across the surface of the CCD.

[1] This work is supported by the ESA General Studies Programme
[2] Radiation Effects Group, MBDA UK Ltd., Filton, Bristol, England
[3] ESTEC, Noordwijk, The Netherlands
[4] Marconi Applied Technologies, Chelmsford, Essex, England
[5] Royal Military College of Science, Cranfield University, Shrivenham, England

II. DESCRIPTION

An outline of the CCD Miniature Radiation Monitor design is shown in Figure 1. The pinhole is of the order of a square millimetre and the CCD surface approximately a square centimetre. Electrons and low energy protons can only enter the instrument in the close vicinity of the pinhole, but higher energy protons are sufficiently penetrating to enter via an annulus of the pinhole wall, the radius of which grows with increasing proton energy. Above a certain threshold energy, protons will be able to penetrate the walls of the pinhole cavity. It is essential that a high density (high-Z) shielding material be used, both to minimise the effective area of the pinhole for protons at any given energy and because it may be shown that the mass-efficiency of the shielding is optimal for high-Z metals. The total mass of the cavity is less than 100g.

The surface of the CCD may be covered with relatively thin planar layers of additional high-Z shielding. This "local" shielding serves three purposes:-

a) The electron dose at the CCD surface would be excessively high for most missions in the absence of a minimal layer of local shielding.
b) With several different thicknesses of local shielding the electron dose-depth curve (and a portion of the proton dose-depth curve) may be measured. From this curve it is possible to reconstruct the electron energy spectrum.
c) The CCD surface needs to be protected from sunlight.

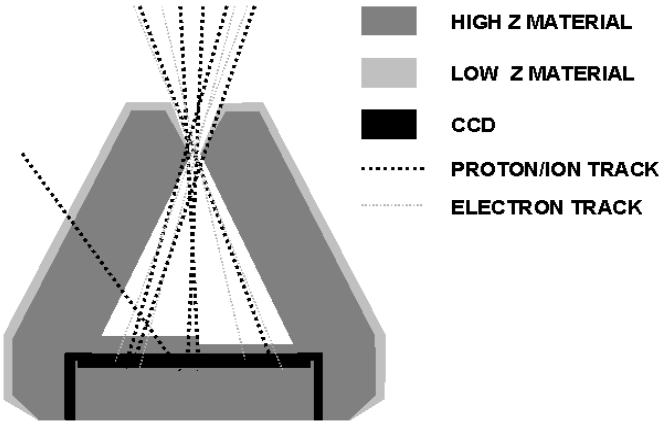

Figure 1: Cross-section through a CCD Miniature Radiation Monitor cavity.

The thin outer coating of low-Z material is a precaution against excessive bremsstrahlung generation.

Since the cavity is conical and the CCD is rectangular, the corners of the array will be deeply ensconced in the walls of the cavity. Only very high energy protons will reach these

pixels. The ratio of the proton hit rate in the corner pixels to that in the centre of the array provides a good measure of the hardness of the ambient proton spectrum.

III. Data Analysis & Resolution

A typical array would normally comprise >1E5 pixels. The frame rate might be up to 10Hz in practice. The data rate in these frames would therefore be at least a megabyte per second. Transmission of this amount of data to the ground station would be impractical for most missions. Furthermore, there is little point in transmitting information at pixel scale resolution, since the directional resolution at the array surface cannot exceed the effective area of the pinhole. The instrument must therefore possess an appropriate data analysis and compression capability.

In view of the pinhole area constraint on the directional resolution it is appropriate to divide the array surface into blocks of pixels of area comparable to the area of the pinhole - perhaps 10 x 10 such elements (Figure 2). Each of these Radiation Image Elements (RIE's) comprises around several thousands of CCD pixels.

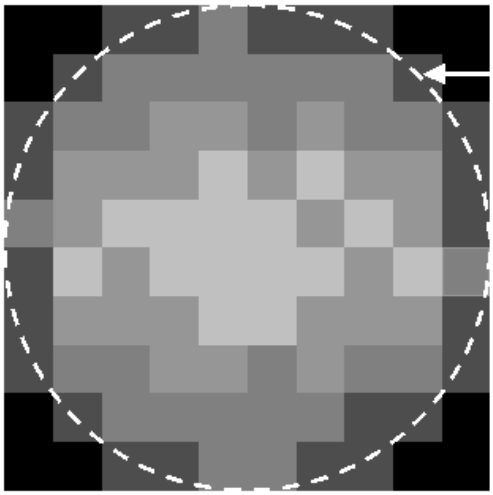

Figure 2: The division of the array into large radiation image elements (greyscale conceptually represents radiation intensity).

A radiation image for both the proton and the electron radiation fields needs to be generated. Since each image requires about 100 bytes, the data rate is reduced to around 2kbytes per second for a 0.1 second frame rate. Furthermore, occasional ion strikes should be discernible in the proton field image as RIE's with exceptional proton counts, since it is found [2] that ions produce large comet-like clusters of saturated pixels.

A relatively simple algorithm is feasible for the analysis of the pixel data to generate the proton and electron RIE's. This is predicated on the (realistic) assumption that very few pixels see proton hits within any single integration time. The first step is to count the number of pixels in each RIE, which record a signal level above a pre-defined Proton Counting Threshold (PCT). This count in itself provides a good measure of the proton radiation intensity and can be used directly to generate the proton RIE. The average excess signal (above the mean noise) in the remaining pixels can then be used to define the electron RIE.

There are however some important qualifications upon this algorithm. Firstly, the number of electron hits per pixel per integration time also needs to be <<1, else multiple electron strikes on single pixels will mimic proton hits. Secondly, the LET's (and therefore the pixel signal depositions) of high energy protons fall to levels comparable with very low energy electrons. In practice the optimum strategy will normally be to set the PCT sufficiently high as to count only lower energy protons, then to use the proton spectrum information (derived from the corner RIE's) to infer the relative numbers of high energy protons and thereby make allowance for them.

This algorithm has been implemented in software and validated by applying it to image frames from a Marconi Applied Technologies CCD 02-06 device, which was irradiated using an MeV electron beam. An example CCD frame is shown in Figure 3. The inhomogeneous radiation distribution in this frame qualifies it as a suitable test case.

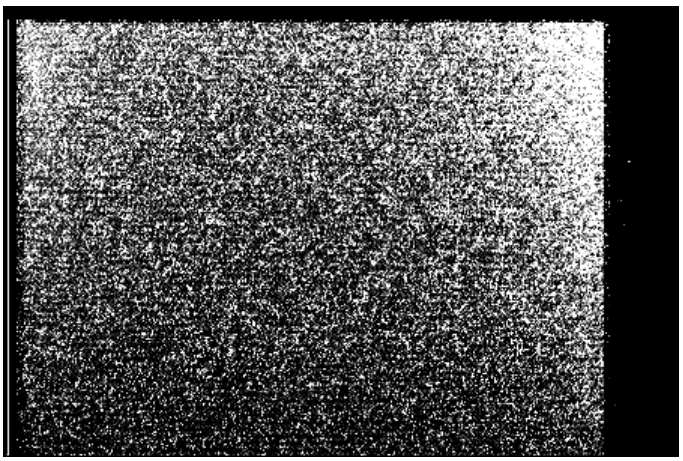

Figure 3: CCD 02-06 frame during irradiation by MeV electrons.

Electron and proton radiation field images for this frame are represented as bar graphs in Figures 4 and 5 respectively. The proton hits were obtained simply by lowering the PCT such that some low energy (high LET) electron hits and multiply struck pixels were counted as proton hits by the software. Note that the variations in the radiation image intensity are far more marked in the "proton" than in the "electron" image. This reflects the higher probability of multiply struck pixels in the more heavily irradiated portions of the array and the effect of stripping the most intensely affected pixels out of the "electron" image.

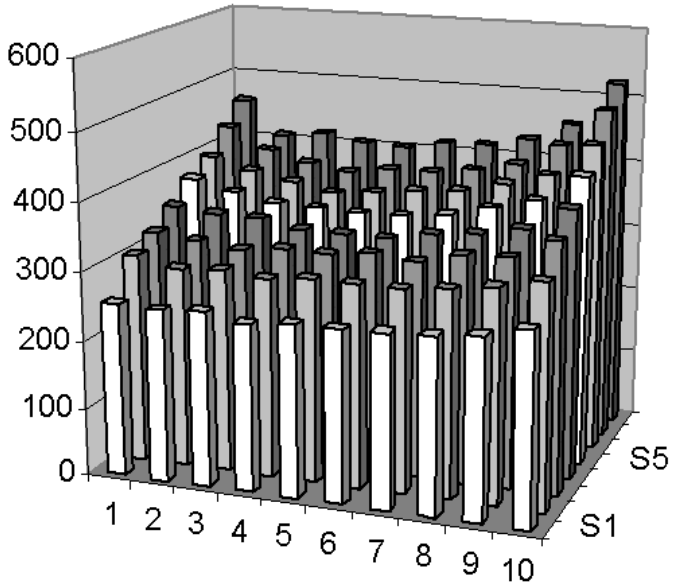

Figure 4: Electron image analysis for the CCD frame (vertical scale is in arbitrary electron dose units).

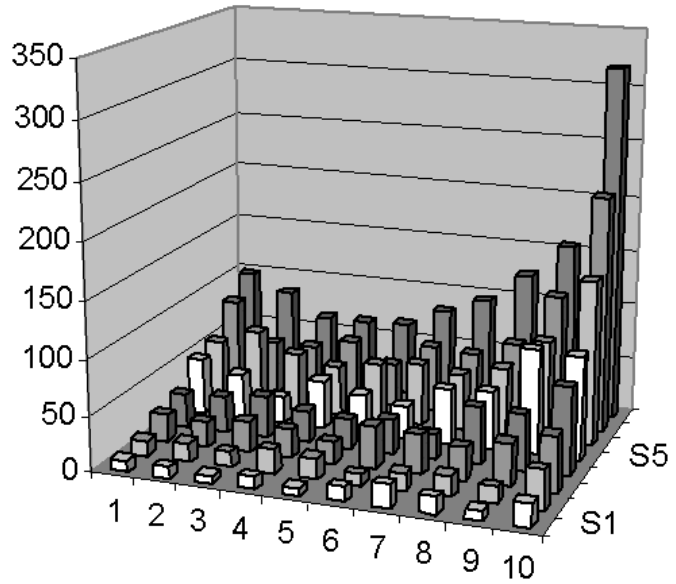

Figure 5: Proton image analysis for the CCD frame (vertical scale is in arbitrary proton dose units).

IV. PROTOTYPE

A prototype CCD MRM has been designed and produced as shown in Figure 6. The local shielding and pinhole cavity components are pictured in Figure 7. This prototype is only designed for testing with radiation beams and radioactive foils (Figure 8), so thick back-shielding is not required. The chosen CCD is an 02-06 device (with IMO technology to minimise dark current accumulation) by Marconi Applied Technologies.

The pinhole cavity has been fabricated with a cone apex angle of 60^{o} using a platinum-iridium alloy. This cavity is 8mm tall with a maximum diameter of 23mm and a mass of 45g. The local shielding is made of 8mm diameter discs of tantalum and is 0.25mm thick on one side and 0.15mm thick on the other. Platinum-iridium alloy is considered the best material for the cavity, since it gives the shortest proton ranges (excepting osmium, which reacts with oxygen), but tungsten would be a less expensive alternative. Many high density metals are viable for the local shield.

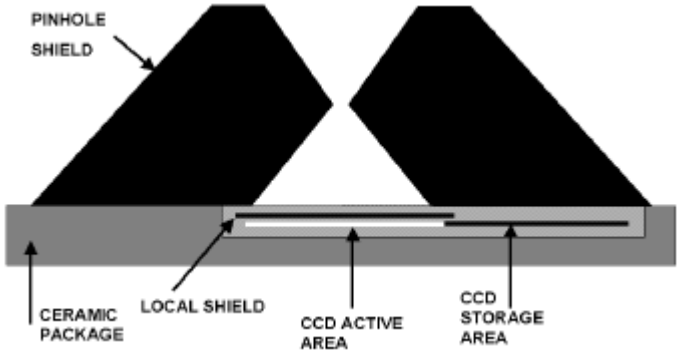

Figure 6: The prototype CCD MRM.

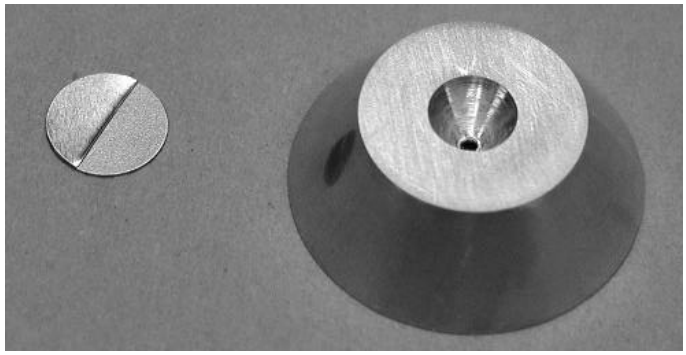

Figure 7: The prototype local shield and pinhole cavity.

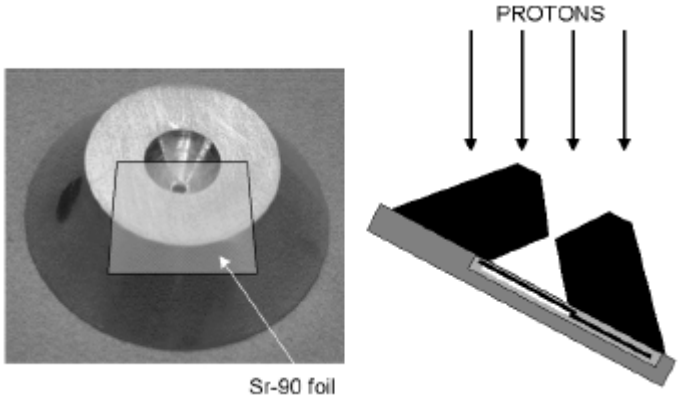

Figure 8: Testing the MRM prototype with a Strontium-90 foil and with a proton beam.

A test and evaluation camera unit provided by the CCD manufacturer was able to run the CCD at a range of frequencies, giving a corresponding range of integration times. In practice, a frequency of either 500kHz or 200kHz was adopted. Frames were captured and digitised from the analogue output stream of the camera and saved onto a PC hard disk using a Microstar data acquisition processor card. The relative sophistication of these support electronics was dictated by the need to capture entire frames at 12 to 14 bit resolution during prototype testing.

V. ELECTRON TESTING

Electron irradiation was conducted at the Royal Military College of Science (RMCS) using beta decay electrons from a 1cm^2 Strontium-90 foil of total activity 0.26MBq. This is a relatively pure source of beta particles of energy ranging up to 2.26MeV. The integration time was 0.24 seconds or 0.6 seconds. In 0.24 seconds there are 6.24E4 disintegrations/cm^2 in the foil. If the foil covers the aperture, it may be calculated that only around 70 betas are admitted to the MRM cavity from the foil during this time. Of these, only half will penetrate the local shielding to reach the CCD.

It is desirable to reduce the area of the foil which can be seen by the pinhole in order to test the directional resolution of the MRM for electrons. A convenient configuration is that shown in Figure 8, where exactly half the pinhole aperture is covered. This can be arranged symmetrically and orthogonally with respect to the step in the local shielding, so as to give the four quadrant split of the radiation image area shown in Figure 9. The radiation image of the foil in line of sight of the array is in the top half of the frame with the thicker local shielding on the left, whilst the lower half cannot directly see radioactive emission sites.

The image in Figure 9 is formed by merging four separate 0.24s frames. The edges of the local shield, which overlaps the edges of the radiation image area, are picked out by the visible light seeping around its edges to produce the darker areas in the corners of the frame. However, the spots in the radiation image area are almost all due to beta particles. As anticipated most beta electrons appear in the top right quadrant, with only about a third as many in the top left and just a few spots in the lower half of the radiation image circle. It can be seen that some of the spots are clustered or mutually aligned. This is because the electron tracks wander significantly after entering the local shield: some will be moving almost in the plane of the array and others may pass through the plane of the array several times along their tortuous trajectories. A few (~10%) of the isolated spots are actually noise peaks rather than beta electrons. The radiation spots in the lower two quadrants are either bremsstrahlung electrons or betas scattered in the rim of the pinhole.

The dose ratio between the two upper quadrants (allowing for noise spots and scattered radiation) was found to be 2.98 for this set of frames. The beta spectrum from a Strontium-90 foil is well approximated by the Fermi theory. Fermi found that, if W be the total energy of the beta particle (including its rest mass) in units of m_oc^2, then the probability PdW of the emission in unit time of a beta particle with energy between W and W+dW is:

$$PdW = kf(Z,W)\,pW(W_{b\,\max} - W)^2\,dW \qquad (1)$$

where k is a constant, $W_{\beta max}$ is the end-point energy (2.26MeV + m_e for Y-90) and p is the momentum of the beta particle in units of m_oc ($p=\sqrt{(W^2-1)}$). The Fermi function f(Z,W) takes into account the effect of the Coulomb field of the nucleus upon the emitted beta. It is comprehensively tabulated in various reference works [5]. This Fermi spectrum has been used in an ITS-ACCEPT radiation transport model [6] to predict a dose ratio of 3.2 between the two upper quadrants in this experiment. However, statistical analysis suggests that all the dose in the upper left quadrant was delivered by just 20 electrons, so there is a random error of standard deviation ~3.2/√20=0.7 in the measured ratio for this test. The measurements therefore agree with the theoretical prediction, since 2.98 is within 0.7 of 3.2. A second measurement gave a dose ratio of 3.5 with a standard deviation of 0.5.

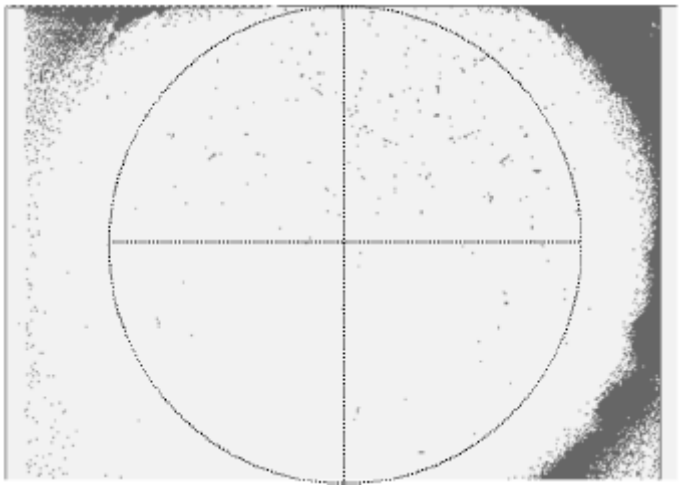

Figure 9: Radiation image (in negative) from 4 merged frames with the Strontium-90 foil half covering the aperture.

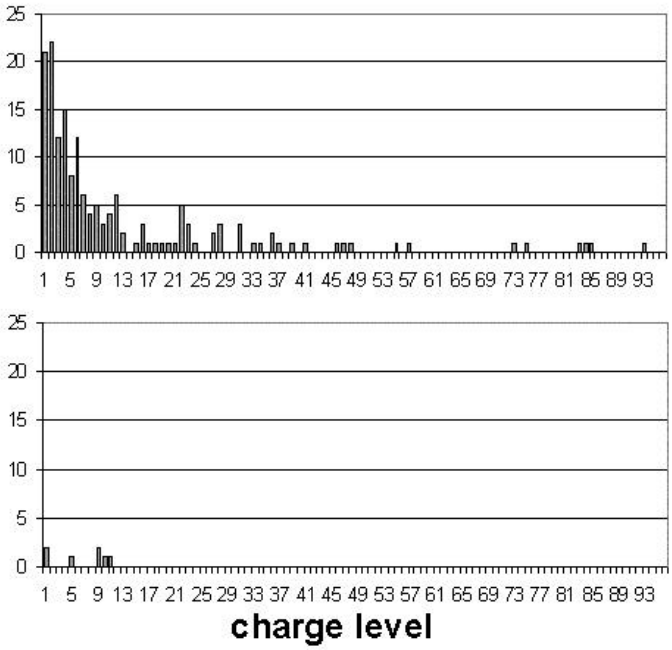

Figure 10: Signal distribution histograms above the noise band for the top right (above) and bottom left (below) quadrants of Figure 9.

The electron deposited signal level distributions in the top right and bottom left quadrants of Figure 9 are plotted in Figure 10. These histograms start from the upper edge of the noise band, which is about 20 units wide on this scale. This upper edge of the noise band has also been used as the cut-off level in Figure 9 (i.e. charge level<1 gives white). The maximum electron signals are just less than 100 units above the noise band (equivalent to around 5000 electron-hole pairs).

VI. Proton Testing

The proton testing of the MRM prototype was conducted at the PSI facility using the PIF beam. Irradiation was performed at a range of proton energies between 18MeV and 300MeV and at a range of beam incidence angles between 0^o and 70^o (Figure 8). The MRM is shown mounted on a stepper motor, so as remotely to adjust the beam incidence angle between irradiations, in Figure 11. The small black box at the right is a video camera, which gave a view down the axis of rotation to verify the incidence angle.

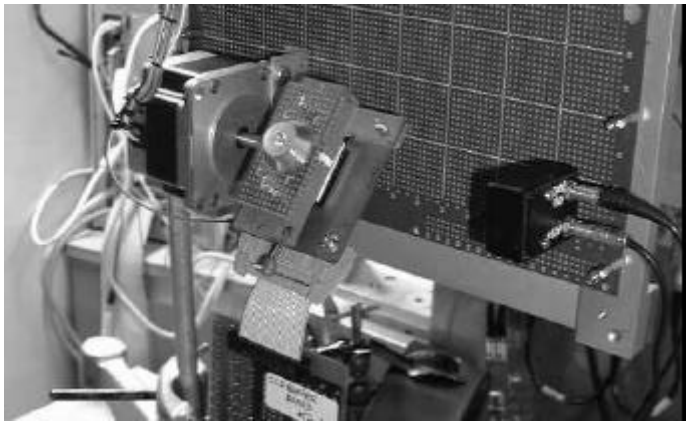

Figure 11: The MRM mounted on a stepper motor at PSI.

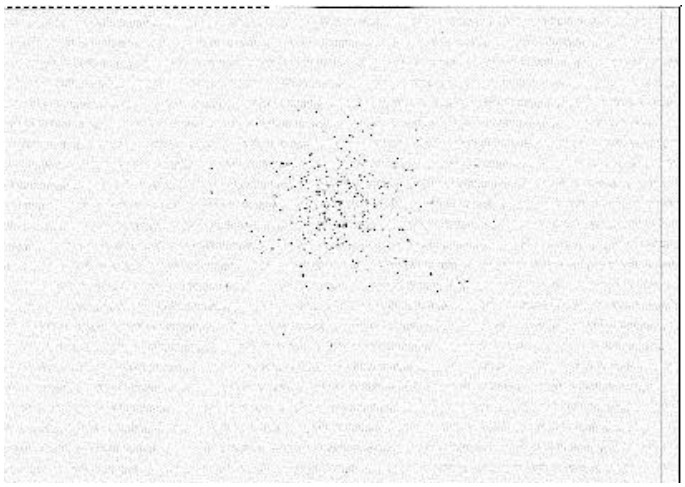

Figure 12: An MRM frame for a 28.1MeV proton fluence of 1.46E4 p/cm^2 at zero degrees incidence (the pinhole was slightly offset from the centre of the array in the vertical direction).

Figure 13: An MRM frame for a 28.1MeV proton fluence of 1.40E4 p/cm^2 at 25.2 degrees incidence.

Two MRM frames captured during 28.1MeV proton irradiation at PSI are reproduced in Figures 12 and 13. The clusters of dark spots are proton hits, whereas the light grey background is noise signal. The external fluences were ~140p/mm^2 delivered in 0.24s in both cases, and this closely matches the spot density at the centres of the clusters, the narrow width of the image area of the CCD being 6.3mm. The spot clusters are essentially projections of the pinhole aperture onto the array. The incidence angle was 0^o for Figure 12 and 25.2^o for Figure 13. The translation of the pinhole projection to the edge of the radiation image area in the second case illustrates and verifies the directional sensitivity of the MRM. The width of the clusters is not much greater than the pinhole diameter (1.1mm) at a few tens of MeV. At higher beam energies the clusters were seen to grow in size in line with predictions as protons penetrated an increasing thickness of the pinhole rim (Figure 14). The theoretical effective aperture diameter is 1.7mm at 28.1MeV and 3.15mm at 60MeV. These figures may be calculated from the proton ranges in the cavity material, which were 0.8mm at 28.1MeV, 3.1mm at 60MeV,

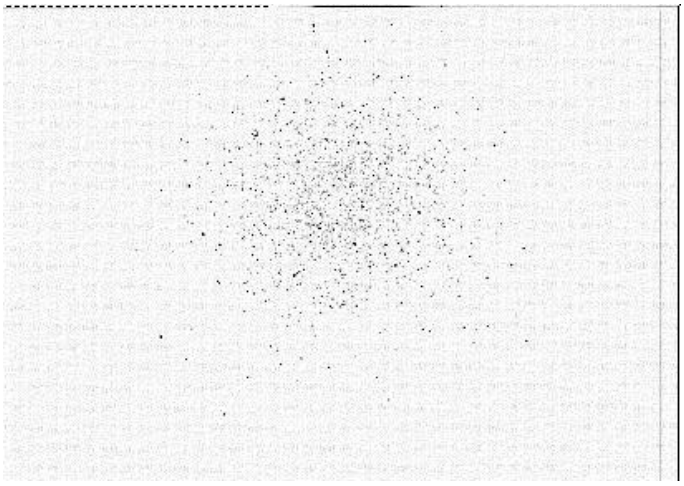

Figure 14: An MRM frame for a 60MeV proton fluence of 2.38E4 p/cm^2 at zero degrees incidence.

7.4mm at 100MeV and 10.1mm at 120MeV. Even at 100MeV blank areas remained in the radiation image, but the whole CCD area saw proton hits at 120MeV as expected.

The results may be further analysed by plotting charge distribution histograms (as for the electrons). An example for the case of 60MeV protons is shown in Figure 15. The upper edge of the noise band occurs at a charge level of around 30 units. The main bulk of the protons hits deposit charge levels between the noise band and around 150 units. These levels correspond to protons reaching the array directly through the pinhole or through thin regions of the rim. They retain most of their initial energy and have a correspondingly low LET. However, protons traversing a larger thickness of rim are reduced to relatively low energies (<10MeV) at the array and have correspondingly higher LET's. These are represented by the hits recorded at hundreds of units in the histogram. These strikes, each depositing tens of thousands of electron-hole pairs, are intense enough to be clearly distinguishable from electron strikes. A few hits (about 30 in this example - represented by the bar at the extreme right) are off the scale above 500 charge units. Some of these are very low energy protons (<1MeV), whereas a few others will be secondaries and recoiling fragments from nuclear interactions of the protons near the array.

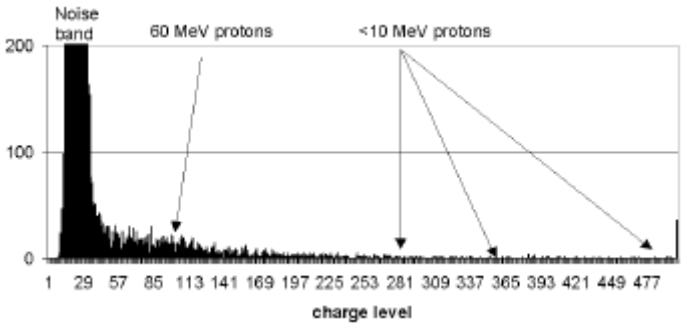

Figure 15: Signal distribution histogram for the radiation image area of an MRM frame with irradiation by a 60MeV proton beam.

The only evidence of radiation damage to the CCD from the proton fluence was that a small number of individual pixels exhibited elevated noise signals, the worst of which were comparable with electron signal levels. These seem to have been due to single event damage clusters, which annealed back towards the noise band on a timescale of hours (and do not therefore pose a significant problem for the performance of the MRM). Only about one in a million protons gave rise to such a damage centre. It is likely that major nuclear interactions occurring in the most sensitive high field regions of the pixels were responsible for these centres, because of their rarity and because they seem to have predominantly been generated by the high energy (>100MeV) proton fluxes.

VII. Future Developments

The next stage of the project is the design and fabrication of a Flight Model of the MRM. This will particularly involve the miniaturisation of the electronics and space qualification of the instrument. Alternative arrays, including single chip digital cameras, and various space-qualified Digital Signal Processing hybrids will be considered for the Flight Model electronics design. It is estimated that the Flight Model will have a power consumption of 100mW for one frame every 10 seconds. When the instrument is flight proven, it would be intended to make it available on a commercial basis.

A preliminary study has also been undertaken into alternative applications of the MRM technology. A higher resolution radiation video camera is feasible with applications in the nuclear industry and a modification of the current design with a smaller pinhole and no local shielding would be sensitive to the low energy electrons of the space plasma environment. Another attractive possibility is the use of an array of MRM devices as an alternative to the scintillator crystal detector arrays in medical gamma camera systems.

VIII. Conclusions

It has been demonstrated that a CCD MRM utilising suitable shielding configurations is capable of simultaneously measuring the intensities, directionalities and spectra of both the electron and proton space radiation environments with a high level of time resolution. Such a device can itself survive the damaging effects of the space radiation environment in most orbits for normal mission durations (years). The low physical volume, mass and power requirements of such an instrument should make it highly desirable as the basis of future spacecraft radiation environment monitoring.

References

[1] AM Chugg & GR Hopkinson, A New Approach to Modelling Radiation Noise in CCD's, IEEE Transactions on Nuclear Science, Vol. 45, No. 3, p. 1518-1523, June 1998.

[2] T S Lomheim et al, Imaging Charge-Coupled Device (CCD) Transient Response to 17 and 50 MeV Proton and Heavy-Ion Irradiation, IEEE Transactions on Nuclear Science, Vol. 37, No. 6, p. 1876-1885, December, 1990.

[3] G R Hopkinson, Proton Damage Effects on P-Channel CCD's, IEEE Transactions on Nuclear Science, Vol. 46, No. 6, p. 1790-1796, December 1999.

[4] Cheryl Dale, Paul Marshall, Brent Cummings, Louis Shamey, Andrew Holland, Displacement Damage Effects in Mixed Particle Environments for Shielded Spacecraft CCD's, IEEE Transactions on Nuclear Science, Vol. 40, No. 6, p. 1628-1637, December 1993.

[5] M E Rose in Beta & Gamma Ray Spectroscopy, edited by K Siegbahn, North Holland Publishing Co., Amsterdam, 1955.

[6] J A Halbleib et al, ITS Version 3.0: The Integrated TIGER Series of Coupled Electron-Photon Monte Carlo Transport Codes, Sandia National Laboratories, USA, March 1992.